REPORT DOCUMENTATION PAGE

AFRL-SR-AR-TR-03-

0366

Public reporting burden for this collection of information is estimated to average 1 hour per response, including the time for revie gathering and maintaining the data needed, and completing and reviewing the collection of information. Send comments regard of information, including suggestions for reducing this burden to Washington Headquarters Service, Directorate for Information 1215 Jefferson Davis Highway, Suite 1204, Arlington, VA 22202-4302, and to the Office of Management and Budget, Paperwork Reduction Project (0704-0188) Washington, DC 20503.
PLEASE DO NOT RETURN YOUR FORM TO THE ABOVE ADDRESS.

1. REPORT DATE (DD-MM-YYYY) 30-00-2003	2. REPORT DATE Final	3. DATES COVERED (From - To) January 2000 to June 2003

4. TITLE AND SUBTITLE
Compression Behavior of High Performance Polymeric Fibers

5a. CONTRACT NUMBER
F49620-00-1-0147

5b. GRANT NUMBER

5c. PROGRAM ELEMENT NUMBER

6. AUTHOR(S)
Kumar, Satish

5d. PROJECT NUMBER

5e. TASK NUMBER

5f. WORK UNIT NUMBER

7. PERFORMING ORGANIZATION NAME(S) AND ADDRESS(ES)
School of Textile and Fiber Engineering
Georgia Institute of Technology
Atlanta GA 30332-0295

8. PERFORMING ORGANIZATION REPORT NUMBER

9. SPONSORING/MONITORING AGENCY NAME(S) AND ADDRESS(ES)
AFOSR/NL
801 North Randolph St
Arlington VA

20031006 076

12. DISTRIBUTION AVAILABILITY STATEMENT
Approve for Public Release: Distribution Unlimited.

13. SUPPLEMENTARY NOTES

14. ABSTRACT
Hydrogen bonding has proven to be effective in improving the compressive strength of rigid-rod polymeric fibers without resulting in a decrease in tensile strength while covalent crosslinking results in brittle fibers. Tensile strength of the PBO/SWNT fiber containing 10 wt% SWNT is over 50% higher than that of the control PBO fibers containing no SWNT. An optically homogeneous solution/dispersion of single wall carbon nanotubes (SWNTs) in oleum has been used to form isotropic films as well as SWNT coatings on polymers. Addition of SWNT increases the crystallization rate of polypropylene by as much as an order of magnitude or higher. SWNT orientation and exfoliation are important in achieving high modulus SWNT/polymer composite fibers. The specific capacitance of the SWNT/activated carbon film is significantly higher than that of the bucky paper.

15. SUBJECT TERMS
Fibers, rigid-rod polymers, compression behavior, carbon nanotubes

16. SECURITY CLASSIFICATION OF:			17. LIMITATION OF ABSTRACT	18. NUMBER OF PAGES 22	19a. NAME OF RESPONSIBLE PERSON
a. REPORT	b. ABSTRACT	c. THIS PAGE			19b. TELEPONE NUMBER (Include area code)

Standard Form 298 (Rev. 8-98)
Prescribed by ANSI-Std Z39-18

Compression Behavior of High Performance Polymeric Fibers

Table of Contents

Compression Behavior of High Performance Polymeric Fibers

Executive Summary:

Hydrogen bonding has proven to be effective in improving the compressive strength of rigid-rod polymeric fibers without resulting in a decrease in tensile strength while covalent crosslinking results in brittle fibers. After this initial study of the effects of covalent crosslinking and hydrogen bonding on compressive strength, the focus of the project was shifted to carbon nanotube/polymer composites. Tensile strength of the PBO/SWNT fiber containing 10 wt% SWNT is over 50% higher than that of the control PBO fibers containing no SWNT. An optically homogeneous solution/dispersion of single wall carbon nanotubes (SWNTs) in oleum has been used to form SWNT isotropic films as well as SWNT coatings on polymers. Addition of SWNT increases the crystallization rate of polypropylene by as much as an order of magnitude or higher. SWNT orientation and exfoliation are important in achieving high modulus SWNT/polymer composite fibers. The specific capacitance of the SWNT/activated carbon film is significantly higher than that of the bucky paper. PAN/SWNT composite fibers with substantially improved modulus than that of the control PAN are have been processed using solution spinning.

Personnel:

Satish Kumar - PI

Byung G. Min – Research Scientist
Sreekumar T. Veedu – Research Scientist
Tao Liu – Research Scientist
Tetsuya Uchida – Research Scientist
Arup R. Bhattacharyya – Postdoctoral fellow

Shawn Jenkins – Graduate student
Michael A. Laton – Graduate student
Tong Wang – Graduate student

Chongfu Zhou – Graduate student
Huina Guo – Graduate student

Meredith L. Frazer – Undergraduate student
Anthony J. Cascio – Undergraduate student
Jason S. Tully – Undergraduate student

Journal Publications:

1.   S. Jenkins, K. I. Jacob, and S. Kumar, "On the effects of hydrogen bonding in rigid-rod polymers", *J. Polym. Sci. (Phys ed.),* **38**, 3053 - 3061 (2000).

2.   S. Jenkins, K. I. Jacob, M. B. Polk, S. Kumar, T. D. Dang , and F. E. Arnold, " Reaction-induced strain in rigid-rod polymeric fibers", *Macromolecules*, **33**, 9060 - 9068 (2000).

3.   S. Jenkins, K. I. Jacob, M. B. Polk, S. Kumar, T. D. Dang, and F. E. Arnold, "Structure, morphology, and properties of methyl pendant PBI and PBZT", *Macromolecules,* **33**, 8731- 8738 (2000).

4.   S. Jenkins, K. I. Jacob, and S. Kumar, "Crosslinking studies in rigid and semi-rigid polymers", in *Heterophase Network Polymers: Synthesis, Characterization and Properties,* editor B. A. Rozenberg and G. M. Sigalov, Taylor and Francis Group Inc., London, p. 181 - 198 (2002).

5.   S. Jenkins, K. I. Jacob, and S. Kumar, "Effect of electron radiation on mono- and di-methyl pendant PBZT fibers" *J. Materials Sci.,* **37**, 2461-2466 (2002).

6.   S. Kumar, T. D. Dang, F. E. Arnold, A. R. Bhattacharyya, B. G. Min, X. Zhang, R. A. Vaia, C. Park, W. W. Adams, R. H. Hauge, R. E. Smalley, S. Ramesh, and P. A. Willis, "Synthesis, Structure, and Properties of PBO/SWNT Composites," *Macromolecules,* **35**, 9039-9043 (2002).

7.   T. V. Sreekumar, T. Liu, S. Kumar, L. M. Ericson, R. H. Hauge, and R. E. Smalley, Single Wall Carbon Nano Tube Films, *Chemistry of Materials,* **15**, 175 - 178 (2003).

8.   A. R. Bhattacharyya, T. V. Sreekumar, Tao Liu, S. Kumar, L. M. Ericson, R. H. Hauge, and R. E. Smalley, "Crystallization behavior of polypropylene / single wall carbon nano tube composites," *Polymer,* **44**, 2373 - 2377 (2003).

9.   T. Liu and S. Kumar, "Effect of Orientation on the Modulus of SWNT Films and Fibers," *Nano Letters*, **3**, 647 - 650 (2003).

10. F. Yang, Y. Bai, B. G. Min, S. Kumar, and M. B. Polk, "Synthesis and Properties of Star-like Wholly Aromatic Polyester Fibers," *Polymer.*, **44**, 3837-3846 (2003).

11. X. Hu, S. Jenkins, B. G. Min, M. B. Polk, and S. Kumar, "Rigid-rod Polymers: Synthesis, Processing, Simulation, Structure, and Properties," *Macromol. Mater. Engr.* accepted for publication.

12. T. Liu, T. V. Sreekumar, S. Kumar, R. H. Hauge, and R. E. Smalley, "SWNT/PAN Composite Film-based Supercapacitor," *Carbon*, accepted for publication.

13. T. V. Sreekumar, T. Liu, B. G. Min, H. Guo, S. Kumar, R. H. Hauge, and R. E. Smalley, "SWNT/PAN Composite Fibers," submitted for publication.

14. T. Uchida and S. Kumar, "Study of SWNT dispersion in polymers using high resolution transmission electron microscopy", to be published.

Patents:

1. F. E. Arnold, T. D. Dang, and S. Kumar, "Liquid crystalline compositions of rigid-rod polymers and Carbon nanotubes", U. S. patent pending.

2. Tao Liu and Satish Kumar, "Supercapacitor having electrode material comprising carbon nanotubes and process for making the same", U. S. patent pending.

3. Sreekumar T. Veedu and S. Kumar, "Highly conducting single wall carbon nanotube films", U.S. patent pending.

The work that has already been published or is in press is summarized below. A more detailed report is given on PAN/SWNT fibers, as this work has not yet been published.

MePBZT and MePBI Fibers:

Hydrogen bonding has proven to be effective in improving the compressive strength of rigid-rod polymeric fibers without resulting in a decrease in tensile strength while covalent crosslinking results in brittle fibers. Crosslinking of pendant rigid-rod polymers were found to have enhanced shrinkage at elevated temperature due to pendant loss. This was a result of stresses generated due to crosslinking. Thermomechanical analysis and wide angle X-ray diffraction have been used to probe the effects of this stress on a macroscopic and atomic level, respectively. These findings, at least in part explain the observed decrease in tensile strength upon crosslinking of rigid-rod polymers. Though not explicitly determined, results also suggest that the application of tension during fiber heat-treatment would hinder crosslinking. Crosslinking was also attempted by electron irradiation. Methyl-pendant PBZT was found to be stable at high electron

dosage even when electron irradiation was carried out at 225 ℃. If one wishes to crosslink rigid-rod polymers via irradiation, systems should be designed specifically containing radiation sensitive moieties.

Methyl-pendant PBI (MePBI) forms intermolecular hydrogen bond while no hydrogen bonding exit in methyl-pendant PBZT (MePBZT). Otherwise, there were no significant morphological differences between the two systems at the micron and nanometer scales. However, compressive strength of MePBI was markedly higher than that of MePBZT and other weakly associating rigid-rod polymers. The improvement in compressive strength is attributed to increased intermolecular association via the formation of intermolecular hydrogen bonds as opposed to any differences in morphology. In general, a trend of increasing compressive strength, as a function of intermolecular association is observed.

PBO/SWNT Fibers

Poly (p-phenylene benzobisoxazole) (PBO) (Figure 1) was synthesized in the presence of single wall carbon nanotubes (SWNTs) in polyphosphoric acid (PPA) using typical PBO polymerization conditions at the Air Force Research Laboratory. PBO and PBO/SWNT lyotropic liquid crystalline solutions in PPA were spun into fibers using dry-jet wet spinning at Georgia Institute of Technology. Tensile strength of the PBO/SWNT fiber containing 10 wt% SWNT is over 50% higher than that of the control PBO fibers containing no SWNT (Table 1). We have been spinning rigid-rod and other high performance polymeric fibers for over a decade. The tensile strength of 4.2 GPa for PBO/SWNT (90/10) was the highest tensile strength achieved under our laboratory spinning conditions and convinced us of the predicted mechanical properties potential of

5

these materials. Synthesis and fiber spinning experiments have been done at three levels (30, 10, and 1 wt% metal catalytic impurity in the SWNTs) of impurity in the SWNTs. At 30% catalytic impurity, continuous fiber could not be drawn. At 10 wt% impurity, fiber could be drawn; however, its mechanical properties were comparable to that of the PBO synthesized and spun under the same conditions. Dramatic improvements in tensile strength were obtained only when SWNTs with about 1 wt% impurity were used. Attempts to disperse nanotubes above 10 wt% concentration are currently in progress. Extensive high resolution transmission electron microscopy in PBO/SWNT (90/10) has not revealed SWNT aggregates or bundles, suggesting that SWNTs were indeed well dispersed in these samples. On the other hand, both oriented and unoriented nanotube bundles have been observed in PBO/SWNT samples containing 15 wt% nanotubes.

Table 1 Mechanical properties of PBO and PBO/SWNT composite fibers

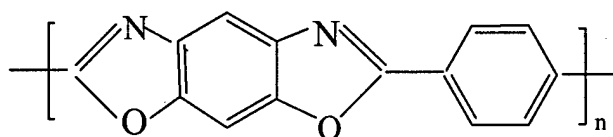| Sample	Fiber Diameter (μm)	Tensile Modulus (GPa)	Strain to Failure (%)	Tensile Strength (GPa)	Compressive Strength (GPa)
PBO	22 ± 2	138 ± 20	2.0 ± 0.2	2.6 ± 0.3	0.35 ± 0.6
PBO/SWNT (95/5)	25 ± 2	156 ± 20	2.3 ± 0.3	3.2 ± 0.3	0.40 ± 0.6
PBO/SWNT (90/10)	25 ± 2	167 ± 15	2.8 ± 0.3	4.2 ± 0.5	0.50 ± 0.6

Figure 1 Chemical repeat unit of PBO

Overall the following spinning trials were done for the rigid-rod /carbon nanotube composite fibers:

Trial #1. (PBZT/SWNT) (95/5). As received HiPCO tubes were used for polymerization. These HiPCO SWNT contained 28 wt% Fe. As received polymer dope was greenish in color and optically homogeneous. Polymer was heated to 120 °C and transferred to spinning cylinder under nitrogen cloud. Polymer solution in the spinning cylinder was heated at 125 °C for one hour. Fiber flowed easily from the spinneret. A wire mesh filter of 51 μm was used. Initially, fiber spinning was attempted at 125 °C. While fiber flowed easily and freely, fiber could not be drawn and taken up continuously. Therefore, fiber spinning temperature was subsequently reduced to 110 °C. This reduction in fiber spinning temperature did not make significant difference in fiber spinnability. Fiber was sent to AFRL for electrical conductivity measurement. Due to lack of significant draw ratio, no mechanical property measurements were conducted on this fiber.

Trial #2. (PBZT/SWNT) (95/5). Purified HiPCO tubes were used for polymerization. The purified HiPCO tubes contained 11 wt% Fe and other non carbon material. The polymer solution at room temperature appeared to be quite rigid. With some difficulty, this polymer was shaped in cylindrical form and transferred to spinning cylinder under nitrogen cloud. Polymer solution was heated to 90 °C for about five hours. Fiber spinning was carried out at 90 °C and at 9 and 15 meters/min. Subsequently, temperature of the polymer solution was raised to 115 °C and fiber was taken up at 9 meters/min. No filter was used. However, high draw ratio could not be obtained at either spinning conditions. Therefore, an attempt was made to do fiber spinning at 80 °C and fiber was once again taken up at 9 meters/min. Spinning draw ratios were rather low and tensile properties of these fibers were poor.

Trial #3. (PBO/SWNT) (95/5). Purity of the HiPCO tubes was greater than 99 wt%. Polymer was preheated to 50 °C for about 15 minutes. This polymer dope was formed into cylindrical shape under dry nitrogen cloud and transferred to the spinning cylinder. Polymer was allowed to heat at 100 °C for about five hours. Fiber spinning went very smoothly and fiber was taken up at 20, 25, and 30 m/min. Fiber was subsequently heated under tension at 400 °C for 2 minutes. A load of 2 grams per fiber was maintained during heat-treatment.

Trial #4. (PBZT/VGNCF) (90/10). Ten weight percent vapor grown nano carbon fiber (VGNCF) from ASI (fiber grade PR-24-HT) was used in polymerization. The as received dope was preheated at about 50 °C. The heated dope was formed into cylindrical shape under dry nitrogen cloud and transferred to the spinning cylinder. The polymer was heated to 100 °C. No filter was used for fiber spinning. Fiber spinning went extremely well. Fiber was collected at 25 and 40 meters/min. While the tensile strength of this fiber was not as high as that for the fiber from trial #3, diameter of this fiber (15 μm) was the lowest achieved during our laboratory spinning and is comparable to the diameter achieved during industrial spinning of high performance fibers.

Trial #5. (PBO). Sample was heated at 100 °C for about 5 hours. Fiber spinning was carried out using dry jet wet spinning at 100 °C. The length of the air gap was 10 cm and length of the coagulation bath was 75 cm. 30 mm spinning cylinder was used with a 28 mm diameter piston. A 50 μm filter was used in line for fiber spinning. Spun fiber was washed in water for one week, vacuum dried at 80 °C for 12 hours and subsequently heat-treated in nitrogen under tension for 2 minutes.

Trial #6. (PBO/SWNT 90/10). The purity of the HiPCO tubes was greater than 99 wt%. The polymer solution was heated to 100 °C. However the fiber could not be spun at this temperature as the thrust was too high. Attempts were also made to spin the fiber at 120 as well as 130 °C. Successful fiber spinning was conducted at 150 °C using dry jet wet spinning. The length of the air gap was 10 cm and length of the coagulation bath was 75 cm. 30 mm spinning cylinder was used with a 28 mm diameter piston. A 50 μm filter was used in line for fiber spinning. Spun fiber was washed in water for one week, vacuum dried at 80 °C for 12 hours and subsequently heat-treated in nitrogen under tension for 2 minutes.

Trial #7 and #8 (PBO/SWNT 80/20 and 85/15). PBO/SWNT dopes in polyphosphoric acid containing 15 and 20 wt% SWNTs were not optically homogenous. However, these fibers could be spun extremely well. However mechanical properties of these fibers was similar or lower than that of the control PBO fiber.

From this rigid-rod polymer/carbon nanotube fiber processing and characterization study, following conclusions can be reached:

- Based on extensive high resolution transmission electron microscopy, SWNT bundles were not observed in PBO/SWNT (90/10), while PBO/SWNT (85/15) contained both oriented and unoriented SWNT bundles (bundle diameter about 15 nm).

- High tensile strength was observed in PBO/SWNT composite fibers utilizing high purity SWNT (SWNT purity greater than 99%).

- High tensile strength PBO/SWNT fibers also did not show the presence of SWNT bundles, suggesting that SWNT exfoliation may also be necessary in achieving high tensile strength fibers.

SWNT Films and Coatings

An optically homogeneous solution/dispersion of single wall carbon nanotubes (SWNTs) in oleum has been used to form isotropic films exhibiting fibrillar morphology. (The micrographs are shown in Figure 2.) Tensile modulus, strength, and strain to failure of the film are 8 GPa, 30 MPa, and 0.5 %, respectively. The electrical conductivity in the plane of the film is 1×10^5 S/m. These dispersions have also been used to develop electrically conducting coatings on polymeric fibers.
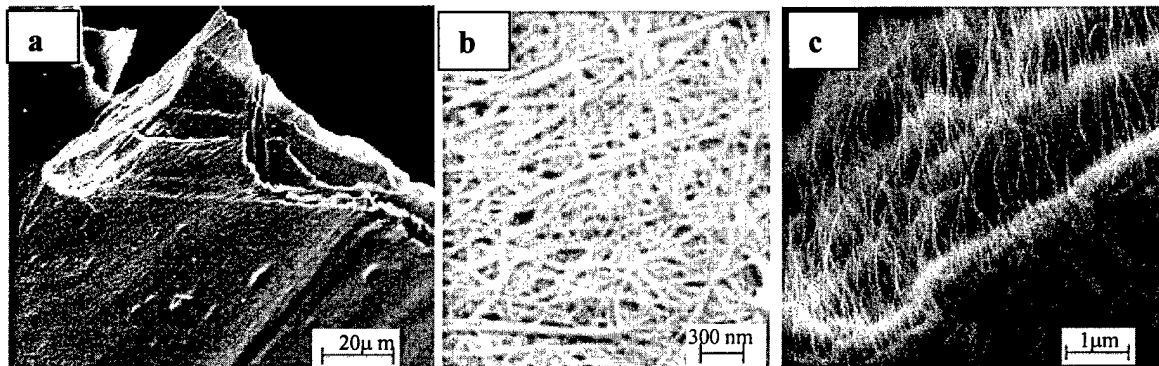

8

Figure 2 Scanning electron micrographs of the SWNT film.

Polypropylene/SWNT Crystallization

We have studied the crystallization and orientation behavior of polypropylene in the presence of SWNTs. Spherulite size in polypropylene is much larger than in PP/SWNT, suggesting that SWNTs act as nucleating sites for polypropylene crystallization (Figure 3). Based on the half crystallization time as a function of isothermal crystallization temperature, one can see that the addition of 0.8 wt % SWNT increases the crystallization rate by as much as an order of magnitude or higher (Figure 4). In the drawn PP/SWNT composite fibers, SWNT orientation was monitored using Raman scattering and that of the PP using X-ray diffraction. These studies show that the orientation of SWNTs (orientation factor 0.95 assuming Gaussian distribution) was higher than that of the PP (orientation factor 0.86).
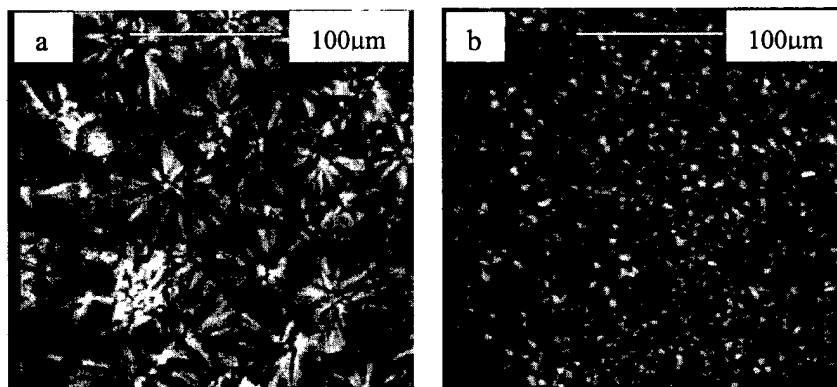

Figure 3 Optical micrographs (with cross-polars) of (a) polypropylene and (b) PP/SWNT composite containing 0.8 wt% SWNTs.
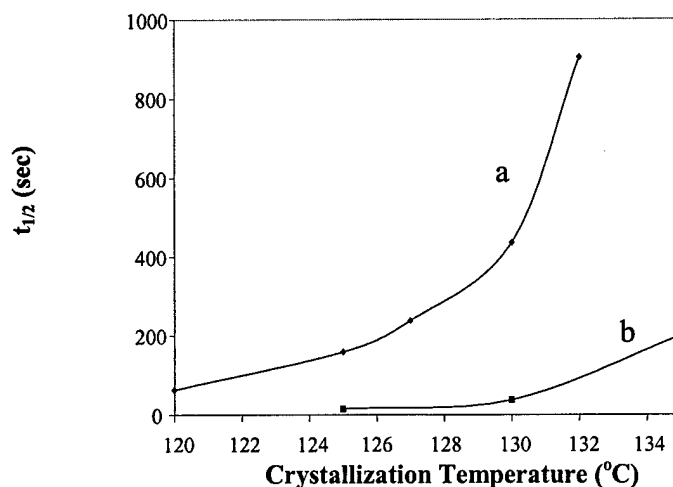
Figure 4 Crystallization half time ($t_{1/2}$) of (a) polypropylene and (b) PP/SWNT (99.2/0.8) as a function of crystallization temperature.

Importance of SWNT Orientation and Exfoliation

Modulus of single wall carbon nanotube (SWNT) films and fibers, calculated using continuum mechanics and the SWNT rope elastic constants is consistent with the experimentally measured moduli of these products. Shear modulus of 20 nm diameter ropes is about 1 GPa, and that of about 4 nm diameter ropes is about 6 GPa. The axial tensile modulus of large diameter ropes drops precipitously with orientation, while the smaller diameter rope modulus exhibit lower orientation dependence (Figure 5). Therefore, in addition to orientation, for the ropes composed of SWNTs with varying diameters and helicity, exfoliation also appears to be important in achieving high modulus SWNT films and fibers.
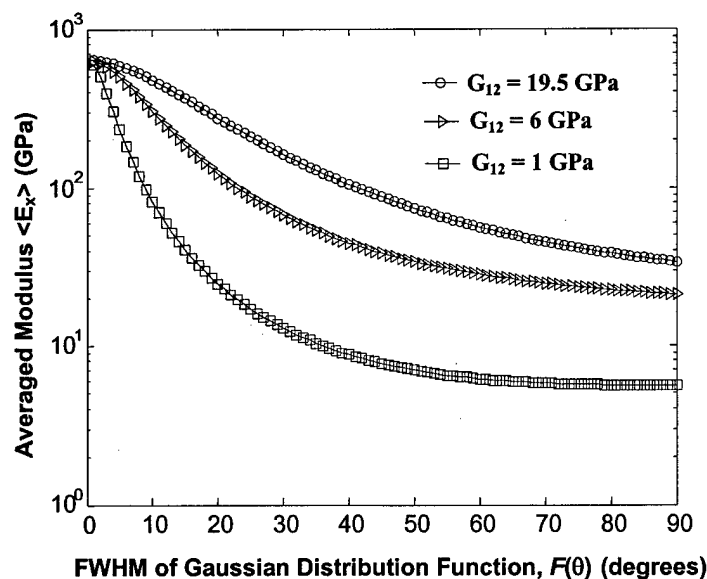
Figure 5 Effect of SWNT rope orientation on the axial tensile modulus of SWNT fiber.

Polymer/SWNT Supercapacitor

Diameter of the as-produced HiPco SWNT ropes used in this study is 35 ± 7 nm and that for the as-prepared SWNT/PAN composite film was estimated to be 57 ± 8 nm. The increased rope diameter indicates PAN copolymer adsorption by the SWNT rope. Physical or chemical activation of polyacrylonitrile or its copolymers is generally used for producing activated carbon with high specific surface area and high porosity, and it is expected that similar activation treatment of SWNT/PAN composite film can also be used for developing SWNT/activated carbon composite films.

The specific capacitance of the SWNT/activated carbon film is significantly higher than that of the bucky paper. The specific capacitance of SWNT/activated carbon at 0.001 ampere discharging current is strongly dependent upon the discharging voltage, a result of its nonlinear discharging behavior. When the discharging voltage is reduced from 0.7 volts to 0.2 volts, the specific capacitance increased from 60 F/g to 380 F/g.

Ragone plot shows that both the power and energy densities of SWNT/activated carbon composite film are significantly higher than that for the SWNT bucky paper.

PAN/SWNT Composite Fiber

SWNTs can be dispersed in solvents such as dimethyl formamide (DMF) and dimethyl acetamide (DMAc) [i,ii]. In this work solution spun PAN/SWNT fibers containing 10 wt% nanotubes exhibit 100 % improvement in tensile modulus (Table 2), significant reduction in thermal shrinkage as well as polymer solubility, and 40 °C increase in glass transition temperature (Figure 6) as compared to the control PAN fiber, suggesting good interaction between PAN and SWNTs. SWNT exhibit higher orientation than polyacrylonitrile as determined by Raman and X-ray diffraction, respectively. SWNT anisotropy in the composite fiber has also been studied using infra-red spectroscopy. Observed modulus of the composite fiber is consistent with theoretical predictions.

The glass transition temperature (Tan δ peak position) increased from ~103 °C for the control PAN fiber to above 143 °C for the PAN/SWNT (90/10) fiber, the magnitude of the tan δ peak decreased significantly, and tan δ peak broadened towards higher temperature (Figure 6a). The motion of PAN molecules closer to the SWNT would be more constrained than those farther away from it. The broadening of the tan δ peak to higher temperatures is attributed to this variation in interaction between PAN and SWNTs. Room temperature modulus of PAN/SWNT (90/10) fiber is nearly twice that of the control PAN fiber, while the modulus retention at 150 °C improved by more than an order of magnitude (Figure 6b).

At 200 °C, shrinkage in PAN/SWNT (90/10) composite fiber is nearly half of the shrinkage in the control PAN fiber (Figure 7). The shrinkage in PAN fiber up to 200°C is mostly entropic. PAN molecules interacting with the SWNTs are not as free to shrink as in the absence of nanotubes. The shrinkage behavior of the composite fibers is consistent with the dynamic mechanical properties data in the sense that both results suggest good interaction between PAN and SWNT. The reduced shrinkage in PAN/SWNT fibers may also be important for carbon fiber processing. Stabilization of the PAN precursor fiber in oxidative environments typically in the 200 to 300 °C temperature range is an important step for the processing of carbon fibers. To obtain high modulus carbon fibers, stabilization is carried out under tension to minimize shrinkage. PAN/SWNT fibers, which exhibit inherently reduced shrinkage, may either reduce the tension requirement or result in fibers with higher orientation and ultimately higher modulus.

Fiber tensile fracture results in significant fibrillation in the control PAN fiber, while the composite fiber exhibited no fibrillation but showed longitudinal splitting. PAN fiber readily dissolves in DMF and DMAc, while PAN/SWNT composite fiber did not dissolve even after several days at room temperature. Rather, it disintegrated into millimeter and submillimeter size particles. The filtered (Fisherbrand Filter Paper, P5) solvent was colorless, suggesting that no nanotubes dissolved. FTIR analysis confirmed the presence of PAN in the solvent. Based on the residual weight analysis, it was estimated that only about 50% of the PAN in PAN/SWNT (95/5) composite fiber dissolved. PAN-SWNT interaction prevents its complete dissolution.

SWNT Herman's orientation factor[1] determined from Raman spectroscopy with 1, 5, and 10 wt% SWNT were 0.90, 0.94, and 0.92, respectively. The SWNT anisotropy was also observed using infra-red spectroscopy (Figure 8). PAN fiber spectra for the two polarization directions are comparable, while the composite fiber spectra with 1 wt% nanotube show significant difference in the two polarization directions. For the 5 wt% nanotube fiber, absorption even for the perpendicularly polarized beam was very high and no transmitted beam could be observed. The SWNTs show much higher absorption when the electric field of the incident wave is parallel to the tube axis. This absorption behavior of SWNTs can be used to develop polymer/SWNTs composites with tailored absorption characteristics for the electromagnetic waves, particularly at low SWNT concentration (<1 wt%).

WAXD showed no diffraction peaks corresponding to SWNTs. The crystallite size from (1, 0) PAN equatorial peak determined using the Scherrer equation [iii], was 5.6 nm, for PAN as well as for the 5 and 10 wt% composite fibers. From the azimuthal scans (at $2\theta = 16.8^0$), the Herman's orientation factor for the (1, 0) diffraction peak was determined to be -0.29, -0.34, and -0.33 for the PAN, and 5 and 10 wt% composite fibers, respectively. Based on this [iv] PAN orientation factor along the chain axis can be estimated to be 0.58, 0.68, and 0.66 for the PAN, 5 and 10% PAN/SWNT fibers, respectively. A comparison of orientation factors show that in the composite fiber, SWNTs have higher orientation than PAN. This is attributed to higher rigidity and lower relaxation times for SWNTs as compared to PAN.

---

[1] Herman's orientation factor (*f*) is given by $f = \dfrac{3 < cos^2 \theta > -1}{2}$, where θ is the angle between SWNT and the fiber axis.

Now we consider the reinforcement efficiency of SWNTs. Mechanical properties of a two-phase composite, in which both the matrix and the reinforcement have different orientation [v], requires full set of elastic constants for the anisotropic matrix, which are currently not available for PAN. Therefore the composite fiber modulus (E_c) was estimated using the equation,

$$E_c = V_{NT}E_{NT} + V_{PAN}E_{PAN},$$

where, E_{NT} and E_{PAN} are the nanotube and PAN moduli along the fiber axis, and V_{NT}, and V_{PAN} are their volume fractions, respectively. Based on the SWNT orientation factors for 5 and 10 wt% composite fibers, and the orientation dependence of the SWNT modulus, E_{NT} values obtained from ref [vi] for two different rope diameters are listed in Table 3, along with values of E_{PAN}, V_{NT}, and V_{PAN}. Table 3 shows that the experimental values are well within the predicted modulus range for the two rope diameters. Rope diameter for the SWNT powder used in this study was measured to be 37 ± 8 nm. However, the measured modulus is closer to the predictions based on smaller diameter (of the order of 4 nm) ropes. This suggests that some SWNT rope exfoliation has occurred during mixing, fiber processing, and fiber drawing.

SWNTs dispersed in PAN using typical PAN solvents (DMAc or DMF), have been processed into PAN/SWNT composite fibers. At 10 wt% SWNT, the room temperature fiber modulus improved by a factor of two, while the modulus retention at 150 °C improved by an order of magnitude. Fiber shrinkage at 200 °C was 24% in PAN and 10% in the PAN/SWNT (90/10) fiber. The improved modulus and reduced shrinkage may be important in developing higher modulus PAN based carbon fibers as well as for developing porous carbon structures for

numerous other applications including charge storage and filtration. The glass transition temperature at 10 wt% SWNT loading increased by 40 °C and the Tan δ peak broadened towards higher temperature. As compared to PAN, PAN/SWNT composite fibers exhibit poor solubility. When processed under similar conditions, PAN in PAN/SWNT composite exhibited higher orientation than in the control PAN fiber. In the composite fiber, SWNT exhibited much higher orientation than PAN. SWNT anisotropy was also observed by infra-red spectroscopy. Tensile fracture of the control PAN fiber exhibited fibrillation, while PAN/SWNT fibers failed by longitudinal splitting and showed complete lack of fibrillation. Observed composite fiber modulus is consistent with the theoretical predictions.

Experimental: Purified HiPco SWNTs [vii,viii] exhibiting 7 wt% residue at 800 ^{0}C in air produced at Rice University, and DMF, DMAc as well as Polyacrylonitrile-co-methyl acrylate [P(AN/MA] copolymers obtained from Sigma-Aldrich were used as received. The P(AN/MA) copolymer ratio is 90:10 and the polymer molecular weight is ~ 100, 000 g/mol. SWNTs vacuum dried at 110 °C for 5 hrs were mixed with excess solvent (DMF or DMAc) and sonicated at room temperature for two hours using a bath sonicator (Cole-Parmer 8891R-DTH). During the sonication, the SWNT/solvent mixture was stirred periodically using a bio-homogenizer (Biospec Products Inc. M133/1281-0). The solution/dispersion was then transferred to a round bottom flask, and the excess solvent was boiled off to obtain the desired final SWNT/solvent volume to which P(AN/MA) copolymer was added while stirring at ~5 °C. To obtain a 99:1 PAN/SWNT weight ratio, 0.15 g of purified HiPco SWNTs were mixed with 250 ml DMAc. Excess solvent was boiled-off at 166 °C, to obtain a final (SWNT/DMAc) volume of about 107 ml, which weighs nearly 100 g. This SWNT/DMAc dispersion did not settle for several days, however optical microscopy showed that this mixture was not homogenous. To this dispersion, 14.85 g P(AN/MA) copolymer was added while stirring at ~5 °C. As compared to the SWNT/DMAc dispersion, this P(AN/MA)/SWNT/DMAc dispersion was optically homogeneous, however a few hard SWNT particles

still remained that could not be dispersed. Solutions containing P(AN/MA):SWNT in the 95:5 and 90:10 ratio were also prepared using the same approach. P(AN/MA) copolymer has been referred to as PAN.

The fibers were dry-jet wet spun, on a small-scale spinning machine manufactured by Bradford University Research Ltd, using a singe hole spinneret of 500 μm diameter. A 635 mesh (20 μm) stainless steel filter pack (from TWP Inc.) was used in the spinning process. The dope temperature was maintained at 80 °C, and the air gap (distance between the spinneret orifice and the liquid surface in the first coagulation bath) was about 5 cm. The volumetric throughput rate was 0.27 ml/min/hole to obtain a linear jet velocity <V> of 1.38 m/min. The first take up roller speed, V, was 1.40 m/min to give a jet stretch, <V>/V, of nearly equal to 1. The DMAc: water ratios for baths I, II, and III were 60:40, 10:90, and 0:100, respectively. Baths I and II were maintained at 30 °C, while bath III was maintained at 90 °C. No fiber drawing took place in baths I and II, while fiber was drawn 4.6 times in Bath III and allowed to relax (0.94 times) in the subsequent drying process, which was carried out on a hot plate at 120 °C. The maximum achievable draw ratio for pure PAN fiber was 4.3, while fibers containing 5 and 10 wt% SWNT could be drawn to a higher draw ratio. However, for a meaningful structure and properties comparison, all fibers were drawn to a draw ratio of 4.3. PAN and PAN/SWNT fibers were also prepared using DMF giving comparable results.

Fiber tensile and dynamic mechanical properties were determined using Rheometrics Scientific's solids analyzer (RSA III). The gauge length and crosshead speed for the tensile tests were 25 mm and 10 mm/min, respectively. Dynamic mechanical tests were conducted at a frequency of 10 Hz at a heating rate of 5 °C/min. Fiber shrinkage was determined using TA Instruments thermo-mechanical analyzer (TMA 2940) at 0.38 MPa pre-stress. For orientation determination, Raman spectra were collected in the back scattering geometry using a Holoprobe Research 785 Raman Microscope made by Kaiser Optical System, Inc. using 785 nm excitation laser. Spectra were collected in VV configuration, where the polarizer and the analyzer are parallel to each other, and at 0, 5, 15, 30, 45, 60, 75, and 90 degrees to the fiber axis. The SWNT orientation [ix,x] was determined from the peak intensity of the tangential mode at ~1592 cm^{-1} assuming Gaussian distribution for the nanotubes [x,xi,xii]. The polarized infra-red transmission spectra were recorded on a Perkin Elmer FTIR microscope (Autoimage system) with the polarization direction of the incident IR beam parallel and perpendicular to the fiber axis. In order to reduce the surface scattering, a

17

single filament was pressed in KBr powder, to form a pellet for IR spectra collection. Wide-angle X-ray diffraction was obtained on a multifilament bundle on a Rigaku 2D SAXS/WAXS Diffraction System (Rigaku Micromax-007, 45kV, 66mA, λ = 1.54 Å) using a Rigaku R-Axis IV++ detection system. The diffraction patterns were analyzed using AreaMax V.1.00 and MDI Jade 6.1.

Table 2. Properties of PAN and PAN/SWNT composite fibers

SWNT (wt%)	Fiber cross-sectional area (cm^2)	Tensile Modulus (GPa)	Tensile Strength (GPa)	Elongation at break (%)	T_g (^oC)
0	4.4×10^{-5}	7.9 ± 0.4	0.23 ± 0.03	11.6 ± 1.4	100
5	3.9×10^{-5}	14.2 ± 0.6	0.36 ± 0.02	11.9 ± 1.3	114
10	4.9×10^{-5}	16.2 ± 0.8	0.33 ± 0.02	9.7 ± 1.6	141

Table 3. Physical and mechanical properties of SWNT/PAN composite fibers.

	PAN	PAN/SWNT (95/5 wt%)	PAN/SWNT (90/10 wt%)
V_{NT}	0	4.6	9.2
f_{PAN} (x-ray)	0.58	0.68	0.66
f_{NT} (Raman)	-	0.94	0.92
E_{PAN} (GPa)	7.9	9.4	9.1
E_{NT} (GPa) (SWNT rope diameter >20 nm)*	-	28.2	22.2
E_{NT} (GPa) (SWNT rope diameter ~4.5 nm)*	-	149.1	122.6
E_c (GPa) (SWNT rope diameter $\geq$ 20 nm)	-	10.3	10.3
E_{comp} (GPa) (SWNT rope diameter ~ 4.5 nm)	-	15.8	19.5
E_{exp} (GPa)	7.9	14.2	16.2

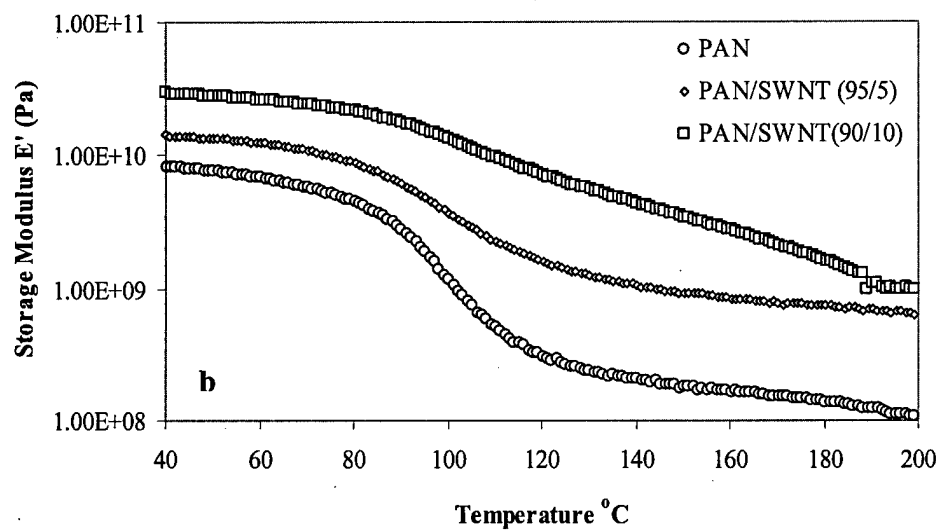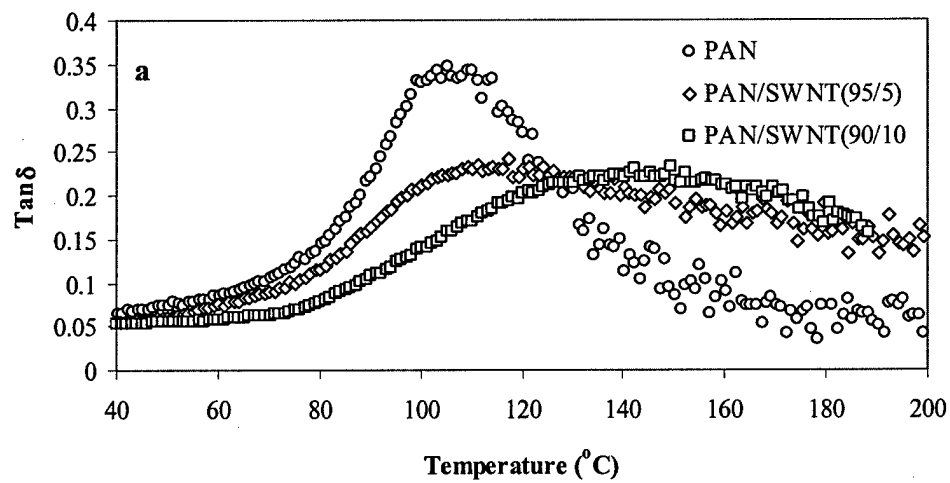*Obtained from ref [vi] for the given f_{NT} and rope diameter.

Figure 6 (a) Tan δ and (b) storage modulus as a function of temperature for PAN and PAN/SWNT composite fibers.
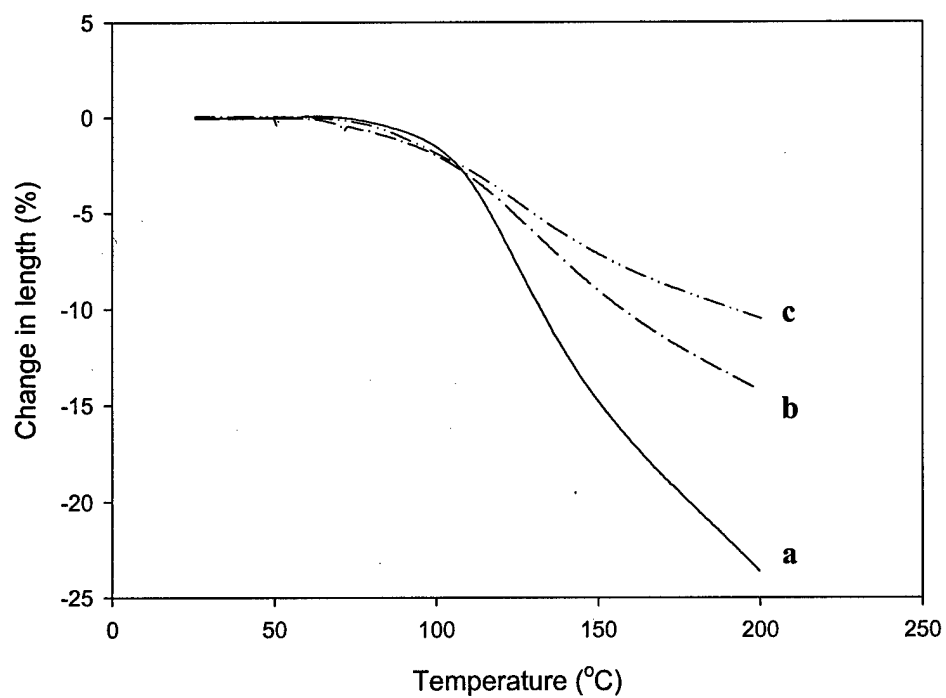
Figure 7. Thermal shrinkage in (a) PAN, (b) PAN/SWNT (95/5), and (b) PAN/SWNT

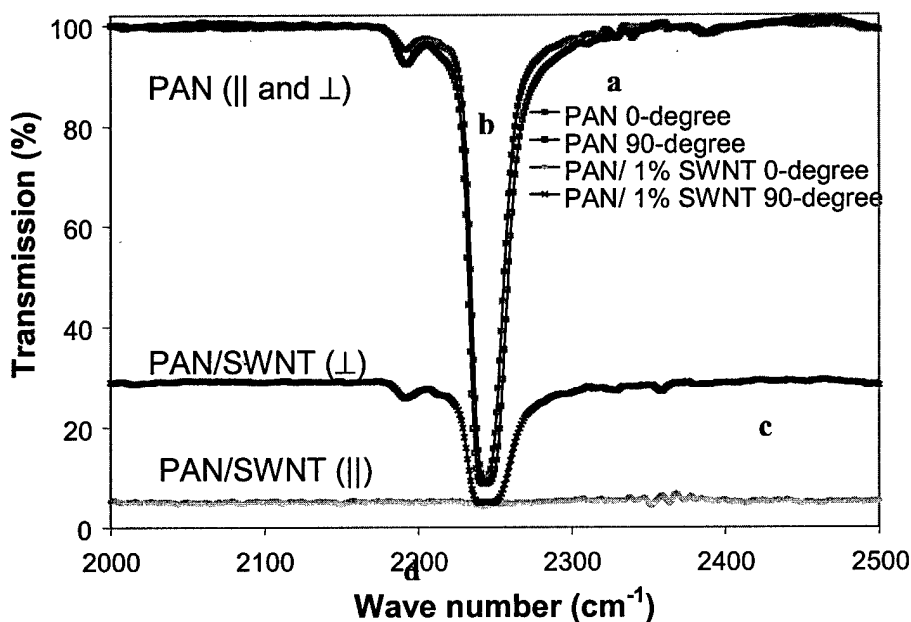990/10) composite fibers as a function of temperature.

Figure 8 Polarized IR spectra of PAN and PAN/SWNT (99:1) composite fibers.

References:

[i] K. D. Ausman, R. Piner, O. Lourie, R. S. Ruoff, M. Korobov. *J. Phys. Chem B.* **2000**, *104*,8911.

[ii] J. L. Bahr, E. T. Mickelson, M. J. Bronikowski, R. E. Smalley, J. M. Tour. *Chem. Commun.* **2001**, *2*, 193.

[iii] B. D. Cullity. Elements of X-Ray Diffraction; Addison-Wesley Publishing Company, Inc. 2nd Ed, 1978; 102

[iv] Samuels, R. J. Structured Polymer Properties: The Identification, Interpretation, and Application of Crystalline Polymer Structure, John Wiley & Sons, New York, **1974**

[v] M. L. Dunn, H. L. Ledbetter, P. R. Heyliger, C. S. Choi. *J. Mech. Phys. Solids.* **1996**, *44*,1509.

[vi] T. Liu, S. Kumar, *Nano Lett. (Communication).* **2003**, *3,* 647.

[vii] P. Nikolaev, M. J. Bronikowski, R. K. Bradley, F. Rohmund, D. T. Colbert, K. A. Smith, R. E. Smalley, *Chem. Phys. Lett.* **1999**, *313*,91.

[viii] I. W. Chiang, B. E. Brinson, R. E. Samlley, J. L. Margrave, R. H. Hauge, *J. Phys. Chem B.* **2001**,*105*,1157.

[ix] R. Haggenmueller, H. H. Gommans, A. G. Rinzler, J. E. Fischer, K. I. Winey, *Chem. Phys. Lett.* **2000**, *330*,219.

[x] J. Hwang, H. H. Gommans, A. Ugawa, H. Tashiro, R. Haggenmueller, K. I. Winey, J. E. Fischer, D.

B. Tanner, A. Rinzler, *Phys. Rev. B.* **2000**, *62*, R13310.

[xi]H. H. Gommans, J. W. Alldredge, H. Tashiro, J. Park, J. Magnuson, A. G. Rinzler, *J. Appl. Phys.* **2000**,

88, 2509.

[xii] J. E. Fischer, W. Zhou, J. Vavro, M. C. Llaguno, C. Guthy, R. Haggenmueller, M. J. Casavant, D. E.

Walters, R. E. Smalley, *J. Appl. Phys.* **2003**, *93*, 2157.